Molecular Catalysis 599 (2026) 116006

Contents lists available at ScienceDirect

Molecular Catalysis

journal homepage: www.journals.elsevier.com/molecular-catalysis

Spectrochemical tuning of Pd(II)dipyrrinato photocatalysts for visible-light mediated oxidative transformations

Shekhar Kumar, Yati [1], Samrita Sharma [1], Anirban Mondal [*], Iti Gupta [*]

Department of Chemistry, IIT Gandhinagar, Palaj, Gandhinagar 382355, Gujarat, India

ARTICLE INFO

Keywords:
Photocatalysis
Dipyrrinato complexes
Aerobic oxidation
Witkop oxidation
Photo-oxidative amide synthesis
Oxidative functionalization of tetrahydroisoquinolines

ABSTRACT

This work is focused on the synthesis of Pd(II)dipyrrinato complexes and their systematic evaluation as visible-light photocatalysts for aerobic oxidative reactions. The Pd(II)dipyrrinato complexes exhibited strong visible-light absorption, effective singlet oxygen quantum yields, long-lived triplet excited states, and suitable redox potentials for photoinduced electron-transfer processes. Among the Pd(II)dipyrrinato complexes, **Pd4** exhibited superior photocatalytic performance under visible light irradiation, utilizing either molecular oxygen or atmospheric oxygen as the terminal oxidant. These photocatalytic systems efficiently catalyzed Witkop oxidation (oxidative cleavage of C2–C3 double bond of indoles with a yield up to 88%) with very low catalysts loading 0.05 mol%. Computational studies revealed that triplet excited state lifetime of **Pd4** is significantly high indicating its involvement in reaction process, while energy profile for the Witkop oxidation reaction suggested the dominance of the energy transfer pathway over electron transfer process. Good to excellent product yield was achieved for photo-oxidative amide synthesis, and oxidative functionalization of tetrahydroisoquinolines with broad substrate scope and high functional-group tolerance, under mild conditions and low catalyst loading (0.1 to 0.5 mol%). This study establishes Pd(II)dipyrrinato complexes, particularly **Pd4**, as efficient and versatile photocatalyst for sustainable aerobic oxidation chemistry.

1. Introduction

Visible-light photocatalysis has emerged as a powerful and sustainable strategy for organic transformations under mild reaction conditions [1–3]. A photocatalyst creates reactive intermediate species through photoinduced electron and energy transfer pathways [4–6]. In case of oxidative transformation, use of molecular oxygen as a green, inexpensive, and atom-economical oxidant has gained significant attention, as it avoids the need for stoichiometric oxidants (*m*-CPBA, 2-iodobenzoic acid (IBX), CrO_3, or Oxone) [7,8] and minimizes side product formation [9–11]. While transition metal photocatalysts based on Ru(II) and Ir(III) polypyridyl complexes have been widely explored [12–17]. However, the high cost, limited availability, and sustainability concerns associated with these noble-metal systems have motivated the search for alternative photocatalysts derived from less expensive or more earth-abundant metals. These limitations demand the development of robust and tunable photocatalysts with strong visible-light absorption, suitable redox potentials, and long-lived excited states.

In this context, palladium dipyrrinato complexes represent an attractive platform for photocatalysis, because of palladium's well-established role in homogeneous catalysis [18]. While Dipyrrinato ligands are highly conjugated, their electronic and photophysical properties can be readily tuned through substitution at the *meso* position [19]. Despite having strong absorption, a long-lived triplet excited state, and an excellent singlet oxygen quantum yield, utilization of metal dipyrrinato complexes as photocatalysts for various organic transformations remains comparatively underdeveloped [20–23]. The strong light-absorbing ability of dipyrrin and the redox versatility of palladium could serve as efficient photocatalysts for oxidative transformations.

The oxidative photocatalytic transformation of nitrogen containing molecules, such as indoles [24,25] tetrahydroisoquinolines [26–28] and the formation of amide bonds [29–32] have significant synthetic importance due to their presence in pharmaceuticals, natural products, and biologically active molecules.

Oxidative cleavage of substituted indoles by Witkop oxidation generates 2-ketoacetanilide derivatives, a key intermediate in the synthesis of a wide range of biologically active compounds [33]. Conventional Witkop oxidation protocols often require transition-metal catalysts,

* Corresponding authors.
E-mail addresses: amondal@iitgn.ac.in (A. Mondal), iti@iitgn.ac.in (I. Gupta).
[1] Equal contributions.

https://doi.org/10.1016/j.mcat.2026.116006
Received 17 March 2026; Received in revised form 25 April 2026; Accepted 26 April 2026
Available online 4 May 2026

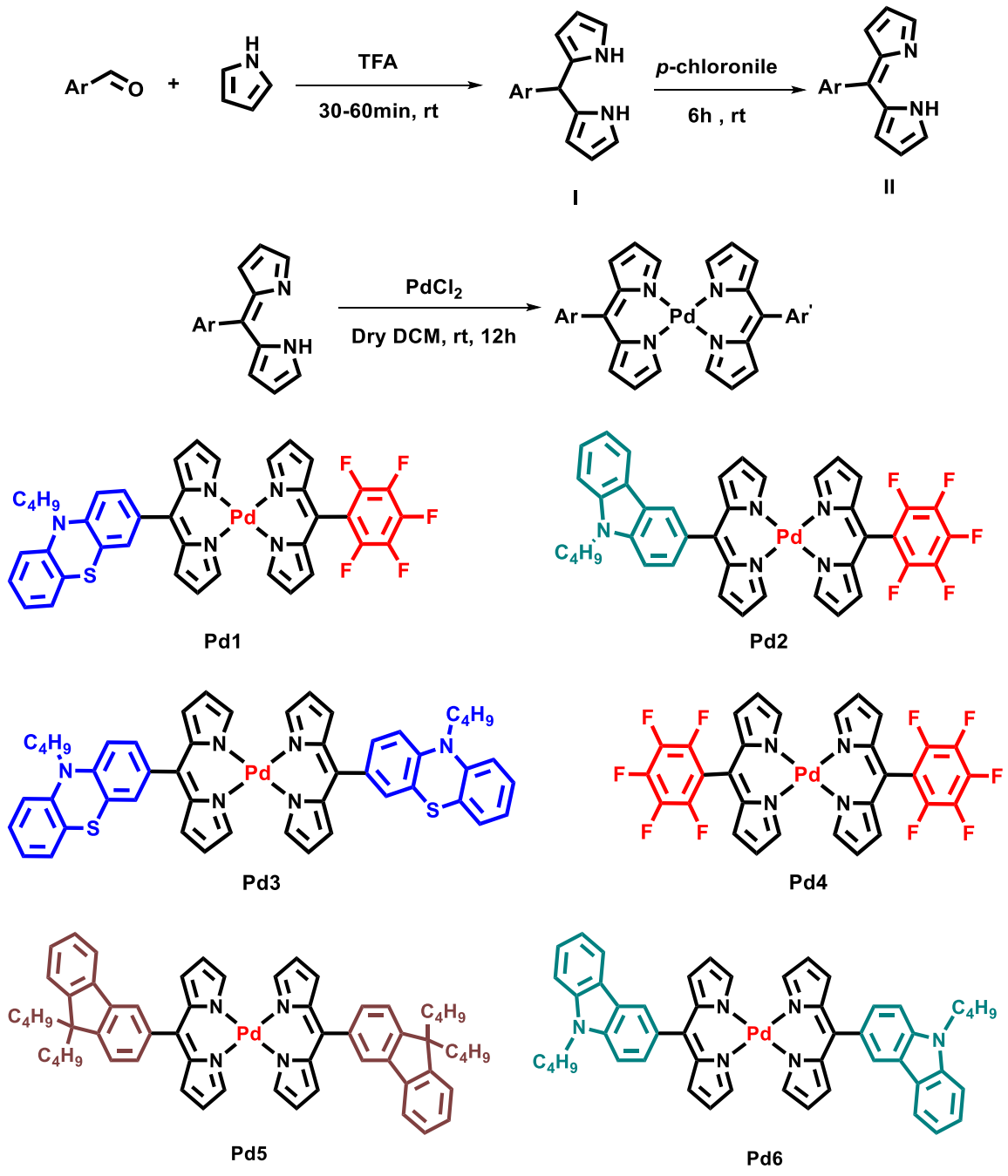

Scheme 1. Synthesis of Pd(II)dipyrrinato complexes.

stoichiometric oxidants, harsh conditions, or toxic reagents, which limit their sustainability [7,34,35]. In the case of amide synthesis, traditional approaches, including activated carboxylic acid and amine couplings as well as the Beckmann rearrangement, Schmidt reaction, and Staudinger ligation, often suffer from poor atom economy due to significant waste generation [36–39]. More recent aldehyde-based oxidative amidation strategies offer attractive alternatives, but they frequently rely on expensive catalysts, harsh reaction conditions, or oxidants other than molecular oxygen, and exhibit limited tolerance toward secondary amines [42–46]. C1-Functionalization of 1,2,3,4-Tetrahydroisoquinolines derivatives was achieved by various methods, including different combinations of catalysts, oxidants, and nucleophiles, but high reaction time, harsh conditions, and the use of stoichiometric oxidants limit its applicability [40–42].

Visible-light-driven aerobic oxidation offers an appealing alternative; however, photocatalysts capable of driving these oxidative reactions under mild conditions [43–52]. Herein, we report the synthesis of a series of Pd(II)dipyrrinato complexes and their photocatalytic ability as visible-light photocatalysts for oxidative transformations. Detailed photophysical, electrochemical and Computational investigations (such as triplet state lifetime and calculation of HOMO-LUMO energy) were performed to evaluate its photocatalytic ability of Pd(II)dipyrrinato complexes. Among the examined Pd(II) dipyrrinato complexes, **Pd4** emerged as a versatile and sustainable method for visible-light photocatalysis, by efficiently carrying out multiple photo-oxidative reactions with low catalytic loading (0.05–0.5 mol%) using molecular oxygen or aerial oxygen as an oxidant. In case of photocatalytic Witkop oxidation reaction mechanistic studies were also

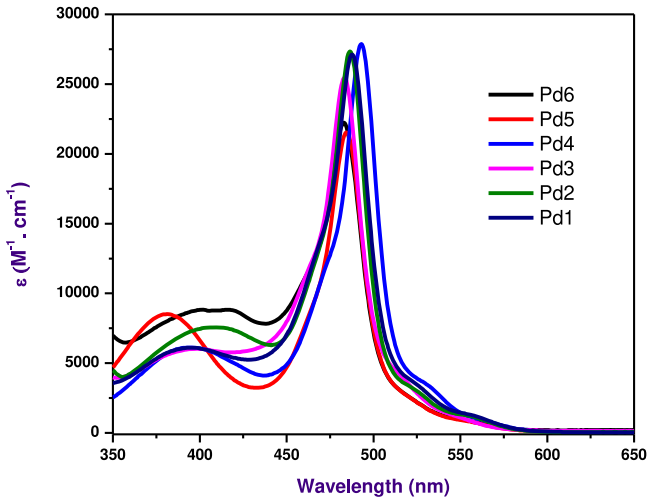

Fig. 1. UV/Vis absorption spectra of Pd(II)dipyrrinato complexes in toluene.

Table 1
Photophysical studies of Pd(II)dipyrrinato complexes.

Complex	Λ_1 (Max)	ε ($M^{-1}\cdot cm^{-1}$)	Λ_2 (Max)	ε ($M^{-1}\cdot cm^{-1}$)	Λ_{em} (Max)
Pd1	488 nm	27,100	395	6100	614
Pd2	486 nm	27,300	409	7580	591
Pd3	483 nm	25,440	399	6040	637
Pd4	494 nm	27,660	395	6120	597
Pd5	484 nm	21,500	381	8520	568
Pd6	485 nm	21,900	401	8820	665

performed which revealed the dominance of the energy transfer pathway over electron transfer pathway.

2. Results and discussions

In this project, a series of Pd(II)dipyrrinato complexes have been synthesized and characterized. Further they have been utilized in various organic reactions, employing molecular oxygen/arial oxygen as the oxidant. The general synthetic pathway for the preparation of Pd (II)–dipyrrinato complexes is outlined in Scheme 1. The dipyrrin ligand precursors were synthesized by following a standard two-step procedure [21] Initially, an acid-catalyzed condensation between pyrrole and the corresponding aldehyde was carried out in the presence of trifluoroacetic acid (TFA) at room temperature for 30–60 min, affording the dipyrromethane **I**. Subsequent oxidation of dipyrromethane **I** using *p*-chloranil for 6 h at room temperature produced the corresponding dipyrrin **II**. In the final step, coordination of dipyrrin ligands to palladium(II) was achieved by treating **II** with $PdCl_2$ in dry dichloromethane at room temperature for 12 h. This reaction furnished the homoleptic Pd (II)–dipyrrinato complexes when identical dipyrrin ligands were used. Alternatively, combining two different dipyrrin ligands under the same conditions resulted in the formation of heteroleptic Pd(II)–dipyrrinato complexes. Using this method a series of Pd(II)–dipyrrinato complexes (**Pd1–Pd6**) were prepared as shown in Scheme 1 by incorporating electron-donating and electron-withdrawing substituents at the *meso* position of the dipyrrin ligands to modulate their structural and electronic properties.

The UV–Vis absorption spectra of the Pd(II)–dipyrrinato complexes (**Pd1–Pd6**) are shown in Fig. 1. All complexes display two characteristic absorption bands. The dominant band appears in the visible region between 450 and 520 nm, arising from the π–π* transition of the conjugated dipyrrinato framework. This transition is responsible for the intense color of the complexes and shows molar absorptivity values in the range of 2.1–2.8 × 10^4 $M^{-1}\cdot cm^{-1}$. Among the series, **Pd4** exhibits the most red-shifted absorption maximum (494 nm), while **Pd3** shows the slight blue shifted peak at 483 nm, reflecting substituent dependent electronic effects on the dipyrrinato ligand π-system.

A high energy second band is observed between 381 and 409 nm, which is assigned to the $S_0 \rightarrow S_2$ ligand-centered transition as shown in Table 1. This band is less intense than the π–π* transition, with ε values between 6.0 × 10^3 and 8.8 × 10^3 $M^{-1}\cdot cm^{-1}$. The normalized fluorescence spectra of **Pd1–Pd6** (Fig. S1) exhibit systematic blue- and red-shifts due to the electronic effects and conformational control of π-conjugation imposed by the *meso*-substituents. Blue-shifted emission was observed for **Pd2, Pd4,** and **Pd5**, whereas **Pd1, Pd3,** and **Pd6** displayed relatively red-shifted emission as shown in Table 1.

The singlet oxygen generation studies were performed for the **Pd4** complex in acetonitrile and chloroform. The standard protocol was used to carry out this assay and Rose Bengal was used as a reference [53]. The plots of the singlet oxygen study in acetonitrile are provided in Fig. 2 for **Pd4** and for other Pd(II)dipyrrinato complexes in Fig. S2. The calculated singlet oxygen quantum yield of **Pd4** was 37% in acetonitrile and 50% in chloroform. Similarly, other Pd(II)dipyrrinato complexes was tested singlet oxygen generation studies they are showing good amount of singlet oxygen quantum yields in both acetonitrile and chloroform data is summarized in Table S1. Electrochemical studies further reveal notable reduction potentials for the Pd(II)dipyrrinato complexes, as summarized in Table 2. The cyclic voltammograms (CV) of Pd(II) dipyrrinato complexes, exhibited well-defined reduction potential in the range of −0.87 V to −1.13 V versus SCE as shown in Fig. S3, where **Pd4** exhibited a potential of –0.96 V versus SCE. While E_{red}* was also calculated using the Rehm–Weller equation [54], the calculated excited-state reduction potentials are positive and quite large (+1.22 to +1.32 V vs SCE), indicating that the excited complexes are strong oxidants in the reaction medium.

The photostability of the Pd(II) dipyrrinato catalyst was evaluated by monitoring its absorbance under continuous irradiation over time shown in Fig. 3. Only a slight and gradual decrease in absorbance was observed, indicating minimal photodegradation and confirming that the catalyst maintains good stability under the reaction conditions.

2.1. Computational methodology

The starting molecular structures of the six Pd-based catalysts were generated using the Gaussian 09 software package [55]. These geometries were used as input for the further density functional theory (DFT) level analysis, performed with the ORCA 5.0.3 quantum chemistry program [56]. For every atom involved, the ground-state geometry optimizations were performed using the B3LYP exchange-correlation functional with the def2-SVP basis set. The geometry optimization runs were performed without symmetry constraints, ensuring that the optimized geometries represent the global minima on the potential energy surface. The electronic structures of the optimized ground-state geometries were analyzed by visualizing and estimating the energy gap between the highest occupied molecular orbital (HOMO) and the lowest unoccupied molecular orbital (LUMO) in the molecule. The Avogadro software package [57] aided the visualization of the HOMO-LUMO distribution on the catalysts. The Multiwfn package [58] was used to calculate the HOMO-LUMO energy gap. Time-dependent DFT (TD-DFT) was used to simulate and analyze the excited-state behavior of the catalysts. The frequency calculations using the NumFreq keyword generated Hessian matrices, which are required for evaluating non-radiative decay pathways and triplet-state dynamics. These Hessian files served as critical inputs for subsequent calculations of excited-state lifetimes. Phosphorescence excited-state decay (PHOSP ESD) calculations were carried out using ORCA to estimate the triplet excited-state lifetimes of the palladium catalysts. These calculations accounted for spin–orbit coupling effects and non-radiative decay processes relevant to phosphorescent transitions.

Finally, we constructed a reaction energy profile for Witkop

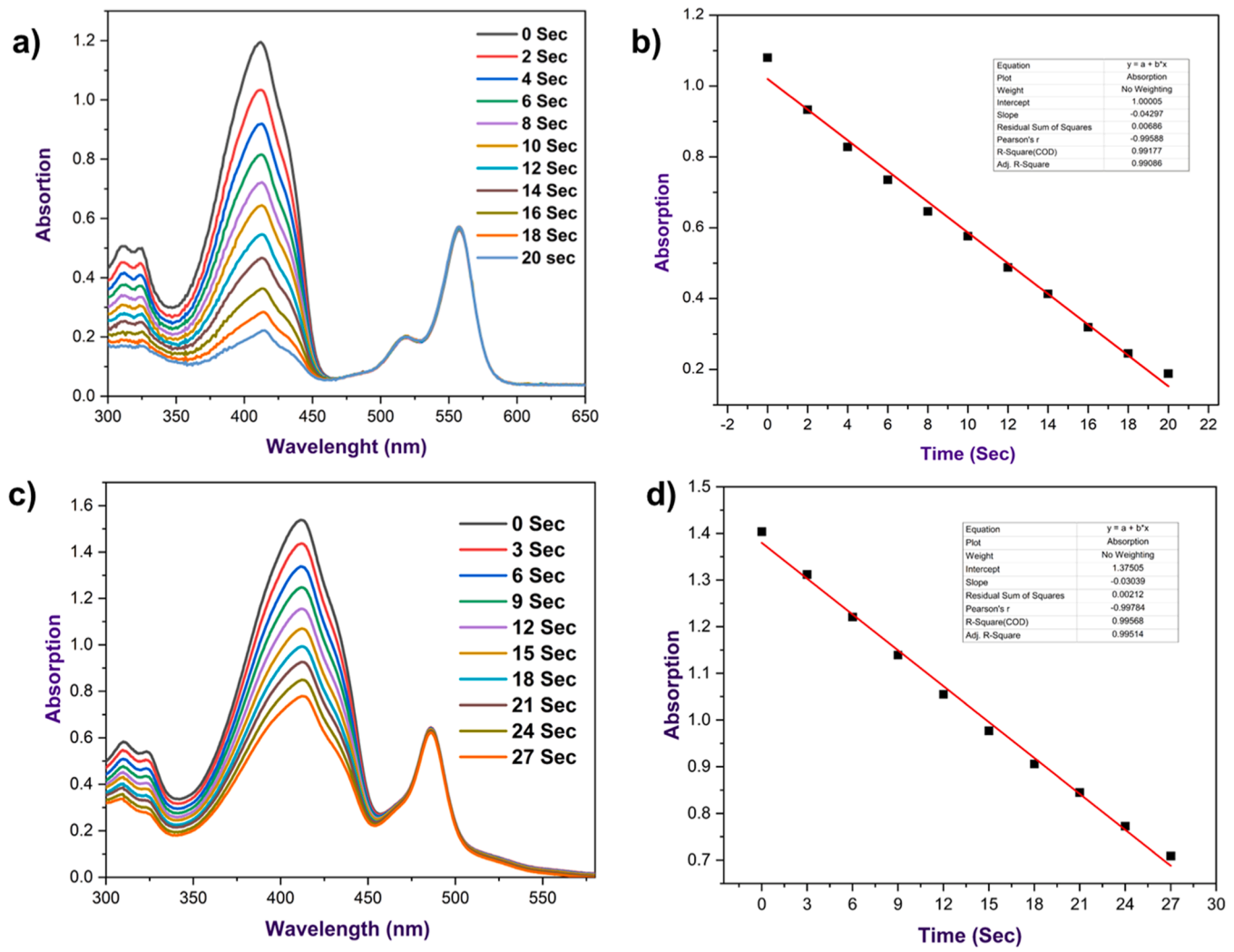

Fig. 2. Singlet oxygen generation experiment, absorption spectra of: (a) Rose Bengal and (c) **Pd4** complex upon irradiation of light (λ = 300–650 nm); rate of decrease of absorbance of DPBF at 400 nm by: (b) Rose Bengal and (d) **Pd4** complex in ACN.

Table 2
Reduction potential of Pd(II)dipyrrinato complexes.

Complex	Reduction Potential (V vs SCE)	$E_{0,0}$	E_{red}*
Pd1	−0.95 V	2.25	+1.30
Pd2	−1.08 V	2.30	+1.22
Pd3	−0.97 V	2.21	+1.24
Pd4	−0.96 V	2.27	+1.31
Pd5	−1.13 V	2.36	+1.23
Pd6	−0.87 V	2.16	+1.29

oxidation with **Pd4** catalyst. This profile was generated using the computed free energies of all relevant intermediates involved in each step of the catalytic cycle, enabling an evaluation of the reaction pathway's energetics and feasibility. The HOMO–LUMO energetics (Fig. 4) of the Pd catalysts govern their roles in photocatalytic oxidation and reduction cycles. Catalysts with higher-lying HOMOs tend to favor oxidative quenching pathways by facilitating electron donation to excited-state acceptors, as observed for **Pd1**. However, excessive HOMO destabilization may compromise the stability of **Pd1**. In contrast, catalysts with low-lying, metal-centered LUMOs such as **Pd3, Pd4,** and **Pd6** are better suited for reductive quenching pathways, enabling efficient electron uptake and transfer. The balanced frontier orbital alignment and metal-centered charge distribution in **Pd4** make it particularly effective for both oxidation and reduction cycles under photoredox

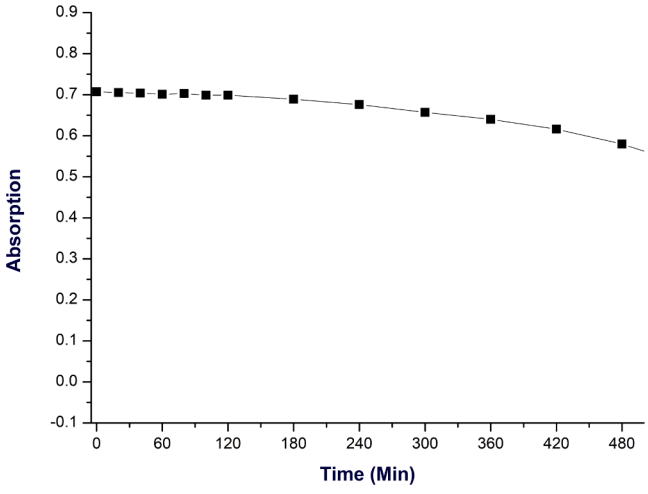

Fig. 3. Time-dependent UV–vis absorption showing photostability of the Pd(II) dipyrrinato catalyst under irradiation.

conditions.The triplet excited-state lifetimes of the Pd(II)dipyrrinato complexes were calculated, and the results are summarized in Table 3.

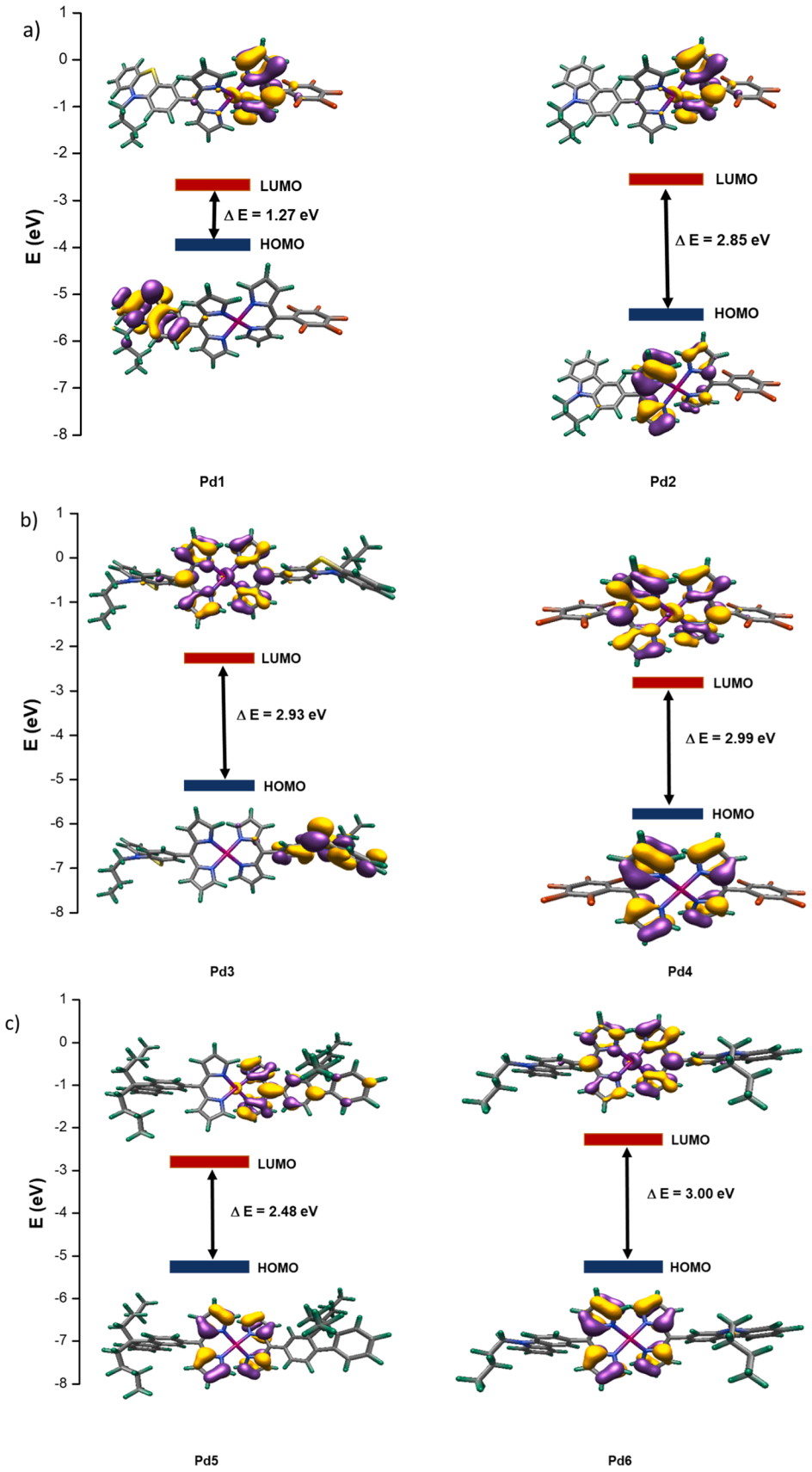

Fig. 4. HOMO–LUMO energy level diagram with orbital isosurfaces a) **Pd1 –Pd2**; b) **Pd3-Pd4; c) Pd5-Pd6.**

Table 3
Computationally calculated excited state lifetime of Pd(II) dipyrrinato complexes.

Complex	Triplet excited state lifetime
Pd1	9.15 ns
Pd2	10,300 ns
Pd3	381 ns
Pd4	15,729 ns
Pd5	190 ns
Pd6	9.91 ns

Table 4
Catalyst optimization for photocatalytic Witkop oxidation[a.]

Sl. No.	Catalyst	% Yield[b]
1	**Pd1**	46
2	**Pd2**	58
3	**Pd3**	26
4	**Pd4**	87
5	**Pd5**	46
6	**Pd6**	14
7[c]	-	6
8[d]	**Pd4**	4

[a] Reaction conditions: 3-methyl indole (0.25 mmol), ACN 4 mL, H_2O 0.4 mL, catalyst (0.05 mol%), K_3PO_4 (0.75 mmol), irradiated with white light (24 W) for 8 h under O_2 at rt.
[b] Yield was calculated by ^1H NMR using 1,3,5 trimethylbenzene (0.25 mmol) as an internal standard.
[c] Without catalyst;.
[d] Without light.

Table 5
Solvent optimization for photocatalytic Witkop oxidation[a.]

Sl. No.	Solvent	Yield[b] %
1	ACN	56
2	DCM	14
3	MeOH	30
4	$CHCl_3$	43
5	THF	39
6	DMF	15
7	H_2O	-
8	DMSO	7
9	ACN + H_2O (10:3)	61
10	ACN + H_2O (10:2.5)	73
11	ACN + H_2O (10:2)	79
12	ACN + H_2O (10:1.5)	82
13	ACN + H_2O (10:1)	87
14	ACN + H_2O (10:0.5)	63

[a] Reaction conditions: 3-methyl indole (0.25 mmol), Solvent 4 mL, catalyst (0.05 mol%), K_3PO_4 (0.75 mmol), irradiated with white light (24 W) for 8 h under O_2 at rt.
[b] Yield was calculated by ^1H NMR using 1,3,5 trimethylbenzene (0. 25 mmol) as an internal standard.

The **Pd2** (10,300 ns) and **Pd4** (15,729 ns) complexes exhibit exceptionally long-lived triplet states compared to the other complexes. Although the Pd(II)dipyrrinato series exhibits effective ground and excited-state redox potentials to carryout photocatalytic transformation, **Pd4** stands out due to its more red-shifted absorption, longest triplet lifetime (15,729 ns), efficient singlet-oxygen generation, and favorable HOMO–LUMO gap. These features collectively make **Pd4** the most effective at activating substrates and molecular oxygen among the series.

2.2. Photocatalytic Witkop oxidation

The long triplet excited state lifetime, efficient singlet-oxygen generation, and strong absorption in visible light with an effective reduction potential motivated us to utilize these molecules for various photocatalytic reactions. Therefore, we initially employed these molecules for the photo-oxidative cleavage of indole. During catalyst optimization, among all Pd(II)dipyrrinato complexes, **Pd4** afforded the desired product in 87% yield, while in other cases, the reaction yield decreased (14%–58%) as shown in Table 4. Solvent screening demonstrated an evident influence of the reaction medium on the Witkop oxidation (Table 5). Among the solvent systems evaluated, acetonitrile yielded a good result (56%), followed by chloroform (43%) and THF (39%). In contrast, protic or strongly coordinating solvents such as MeOH, DMF, and DMSO resulted in significantly reduced efficiencies (7–30%). No product formation was observed in water alone. While, mixed solvent systems of ACN and H_2O enhanced reactivity, with ACN:H_2O (10:3) improving the yield to 61%, and further dilution of water (10:1) delivering the optimal yield of 87%. Further variation in the solvent composition revealed decline in yield, with ACN:H_2O (10:0.5) (10:1.5), (10:2), (10:2.5), and affording 63%, 82%, 79%, and 73%, 61% yields, respectively. This trend suggests that a adequate amount of water facilitates reagent solubility without compromising the behavior of the Pd (II)dipyrrinato catalyst. Overall, the results identify ACN:H_2O (10:1) as the most effective solvent system for enabling efficient photocatalytic oxidative cleavage under the optimized conditions (Scheme 2).

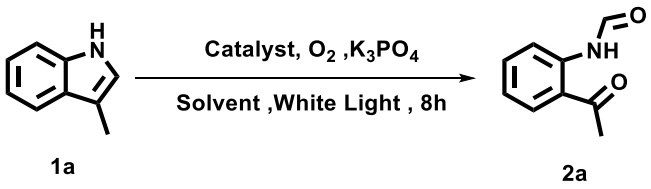

Scheme 2. General scheme of photocatalytic Witkop oxidation of 3-methyl indole.

With the optimized conditions in hand, the substrate scope of the Witkop oxidation was explored (Fig. 5). The parent indole derivative **2a** furnished the corresponding cleavage product in 87% yield, demonstrating the efficiency of the standard substrate. Halogen-substituted indoles were well accommodated, with 5-fluoro (**2b**), 5-chloro (**2c**), and 5--bromo (**2d**) derivatives delivering high yields of 79%, 81%, and 85%, respectively. Phenyl substituted indole also participated in the transformation, though with a comparatively moderate yield **2e** (67%). Electron-withdrawing groups such as acetyl (**2f**, 71%) and fluoro (**2g**, 83%) were tolerated, and excellent yields were obtained for 5-bromo (**2h**, 86%) and 5-chloro (**2i**, 84%) derivatives.

The 3-substituted indole **2j** provided a moderate yield (74%), indicating that substitution at this position is compatible with the reaction manifold. Strong electron-donating substituents, exemplified by methoxy-substituted **2k**, afforded the corresponding product in 88% yield, while CF_3-containing substrate **2l** also reacted efficiently (83%). More sterically demanding frameworks, such as the polycyclic indole derivative gave **2m** with 52% yield. *N*-extended indole substrate such as *N*-benzyl 2,3 dimethyl indole gave **2n** with 60% yield while, in case of *N*-methyl substituted indole derivative gave respective product **2o-2s** with 65%–63% yield. Overall, the scope demonstrates that **Pd4** enables efficient oxidative C–C bond cleavage across a broad range of electronically and sterically diverse indoles.

The role of reactive oxygen species and key reaction components in the photo-oxidative cleavage of indoles was investigated through a series of control and inhibition experiments using specific scavengers (Table 6). The complete inhibition of product formation in the presence of sodium azide, a well-known quencher of singlet oxygen ($^1O_2$), indicates that $^1O_2$ plays a crucial role in the oxidative cleavage process. The addition of benzoquinone, a superoxide radical ($O_2^{\bullet-}$) scavenger, resulted in a significant decrease in yield (17%), suggesting involvement of superoxide species. While there was no significant change in the presence of isopropanol, excluding •OH radical involvement in the

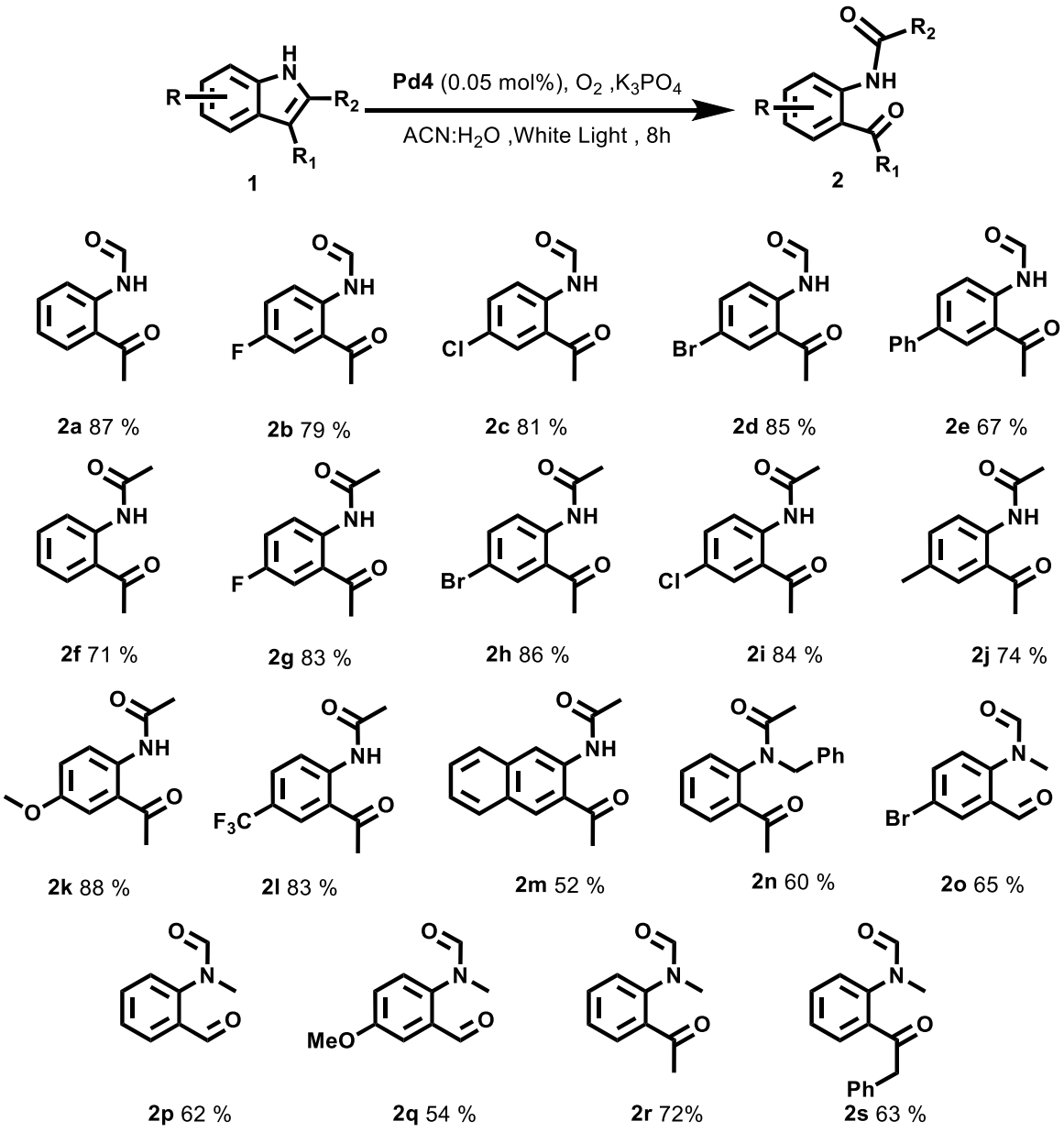

Fig. 5. Substrate scope of photocatalytic Witkop oxidation.

Table 6
Control Inhibition experiments in the presence of various scavengers.[a]

Sl. No.	Scavengers[c]	Inhibited Species	Yield[b] %
1	NaN_3	$^1O_2$	Trace
2	Benzoquinone	$O_2^{\bullet-}$	17
3	Isopropanol	•OH	86
4[d]	No Light	Light	Trace
5[e]	No Catalyst	Catalyst	Trace
6[f]	N_2	O_2	Trace

[a] Reaction conditions: 3-methyl indole (0.25 mmol), ACN 4 mL H_2O 0.4 mL, catalyst (0.05 mol%), K_3PO_4 (0.75 mmol).
[b] Yield was calculated by ^1H NMR using 1,3,5 trimethylbenzene (0. 25 mmol) as an internal standard.
[c] Scavengers (0.25 mmol), irradiated with white light (24 W) for 8 h under O_2 at rt.
[d] No Light.
[e] No Catalyst.
[f] N_2 in place of O_2.

reaction pathway. Control experiments performed in the absence of light, catalyst, or molecular oxygen resulted in no detectable reaction, confirming that visible-light irradiation, the Pd(II)dipyrrinato catalyst, and oxygen are all essential for the photo-oxidative cleavage of indoles.

According to previous work [43], along with control and inhibition experiments, the mechanism of photocatalytic Witkop oxidation is illustrated in Fig. S4. Both electron transfer and energy transfer mechanisms were followed in the reaction. In the case of energy transfer, initially, the photocatalyst becomes excited to the singlet excited state. Through intersystem crossing, it returns to the triplet excited state, which then reacts with the oxygen molecule to produce singlet oxygen. The singlet oxygen reacts with the indole molecule, generating intermediate III, which, upon further rearrangement, yields our Witkop oxidation product. In the case of photo-induced electron transfer, the first excited state of the catalyst reacts with indole, generating Intermediate I, which then reacts with the superoxide radical to form Intermediate II. The superoxide radical was generated by the donation of one electron to oxygen by the cationic radical of the photocatalyst. The Intermediate II gave intermediate III, which, upon further rearrangement,

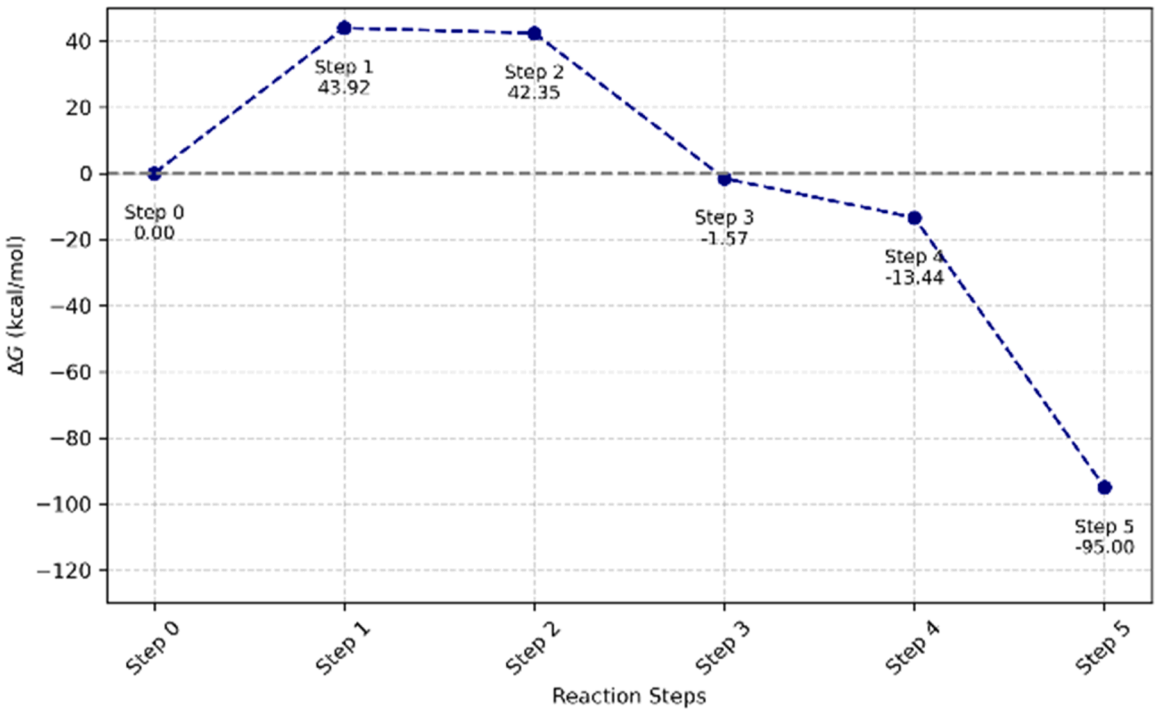

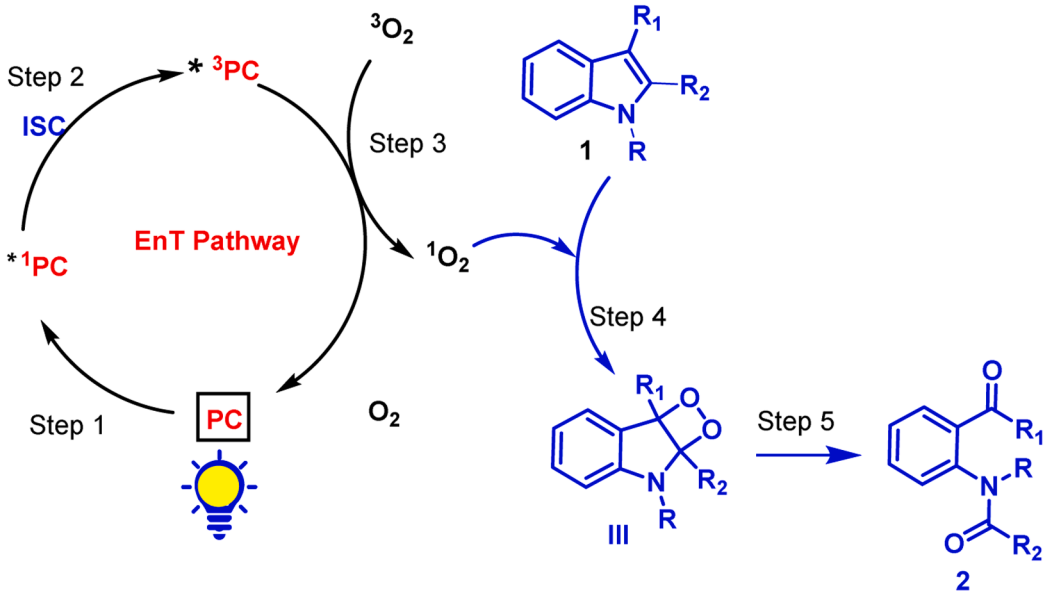

Fig. 6. Reaction profile and mechanism for EnT pathway.

yields the Witkop oxidation product.

To gain further insight into the reaction mechanism, the energy profile for the reaction was calculated using **Pd4** as the photocatalyst. This energy profile for the reaction was generated using the computed free energies of all relevant intermediates involved in each step of the catalytic cycle, enabling an evaluation of the reaction pathway's energetics and feasibility.

In case of the energy-transfer (EnT) pathway, proceeds through the ground-state transformations, as summarized by the reaction profile (Fig. 6). The ground-state catalyst (Step 0) is taken as the reference (0.0 kcal mol^{-1}). Photoexcitation of the catalyst to the singlet excited state Step 1 ($\Delta G = +43.92$ kcal mol^{-1}) and the singlet–triplet energy transfer leads to the formation of the triplet excited state catalyst step 2 ($\Delta G = +42.35$ kcal mol^{-1}). This high-energy region at Step 2, represents the excited EnT intermediate and constitutes the highest point on the profile ($\Delta G = +42.35$ kcal mol^{-1}), identifying it as the rate-determining stage of the EnT pathway. After this point, the reaction becomes strongly downhill. The Pd catalyst returns to the ground state by generating singlet oxygen ($^1O_2$) in step 3 ($\Delta G = -1.57$ kcal mol^{-1}). In step 4 ($\Delta G = -13.44$ kcal mol^{-1}) $^1O_2$ interacts with indole **1** and generates intermediate **III**.

Subsequent structural reorganization and bond formation to the final product further stabilize the system in step 5 resulting in a significant overall stabilization of −95.00 kcal mol^{-1}. In the reaction profile for photo-induced electron transfer (PET) pathway (Fig. 7), the ground state of **Pd4** was taken as reference (step 0). Step 1 corresponds to the

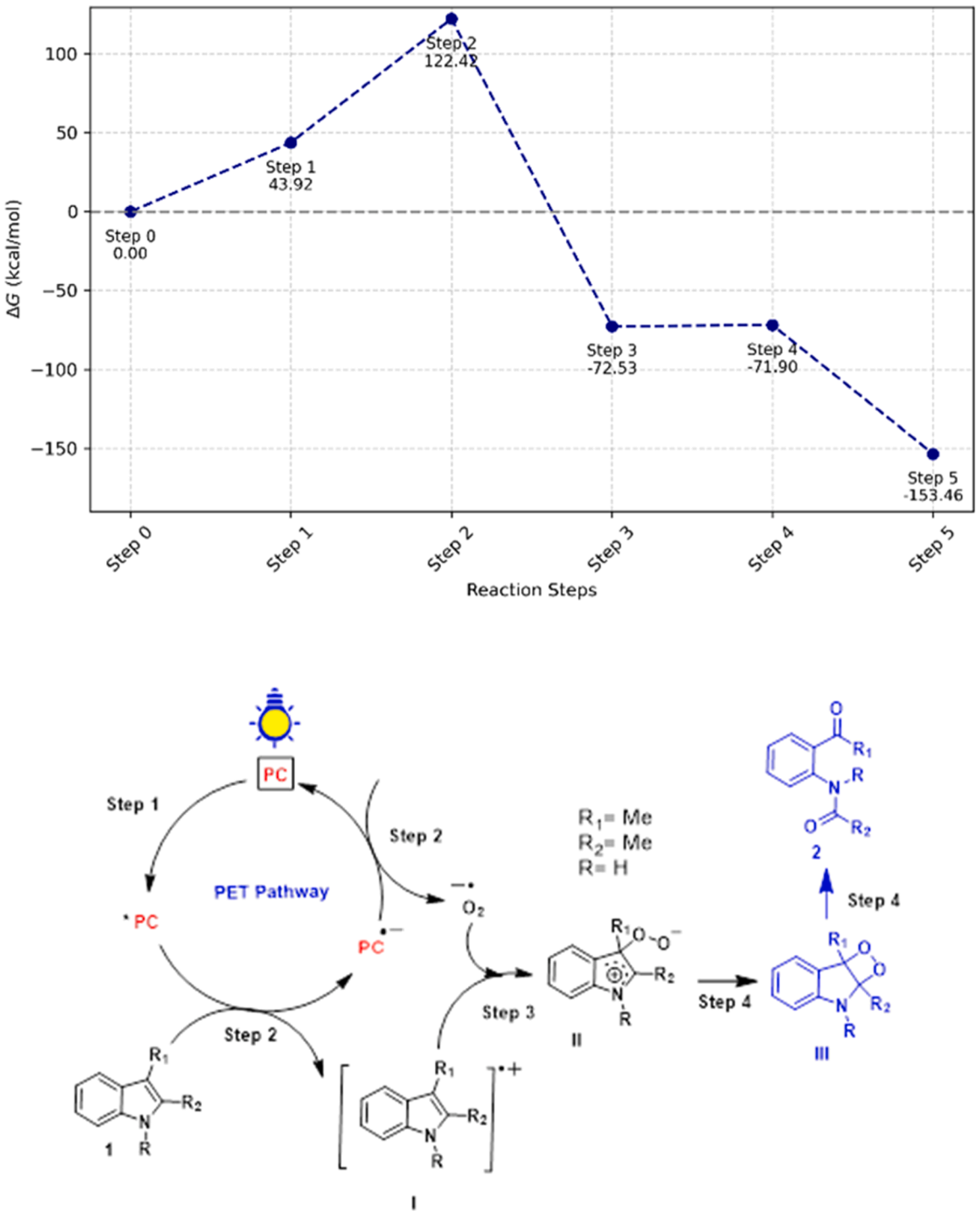

Fig. 7. Reaction profile and mechanism for PET pathway.

formation of the triplet excited state catalyst with an energy of 43.92 kcal mol^{-1}. After that single-electron transfer from indole **1** to the catalyst in Step 2 (ΔG = 122.42 kcal mol^{-1}) to form intermediate **I** and the radical anion of the photocatalyst (**PC•$^-$**) reacts with molecular oxygen, generating superoxide species (O_2•$^-$) along with the ground-state catalyst. In step 3 (ΔG = −72.53 kcal mol^{-1}), intermediate **I** reacts with O_2•$^-$ leading to the formation of a peroxide-type intermediate **II**. The intermediate **II** then undergoes structural reorganization to yield the oxygenated intermediate **III** in Step 4 (ΔG = −71.90 kcal mol^{-1}). Finally, further oxidation and rearrangement afford the final product Step 5 (ΔG = −153.46 kcal mol^{-1}). Compared to the EnT pathway, the PET mechanism involves high-energy charged radical intermediates that are prone to recombination, making it both thermodynamically and kinetically less favorable.

Although EnT is initiated by photoexcitation, it proceeds through a smooth and strongly exothermic energy profile without charge separation, leading to a highly stabilized product. In contrast, the PET pathway requires higher excitation energy and relies on the formation of unstable radical ionic species. Therefore, the EnT pathway can be considered a preferred mechanistic route compared to PET for the photocatalytic Witkop oxidation reaction.

In addition to photocatalytic Witkop oxidation reaction, photo-

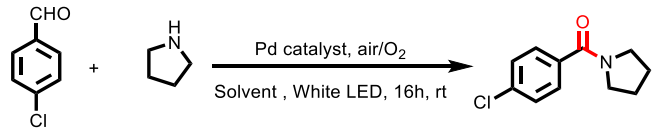

3a 4b

Scheme 3. General scheme of photo-oxidative amide synthesis.

Table 6a
Catalyst amount optimization for photo-oxidative amide synthesis[a].

SL No	Catalyst loading	Yield %
1	0.5	62
2	0.25	61
3	0.1	63
4	0.05	58
5[b]	-	No Reaction

[a] Reaction conditions: 4-Chlorobenzaldehyde (0.25 mmol), pyrrolidine (0.25 mmol), DMF 3 mL, **Pd4**, irradiated with white light (24 W) for 16 h under O_2 at rt.
[b] No catalyst.

Table 7
Catalyst optimization for photo-oxidative amide synthesis[a].

Sl No	Catalyst	Yield %
1	**Pd1**	39
2	**Pd2**	47
3	**Pd3**	38
4	**Pd4**	63
5	**Pd5**	29
6	**Pd6**	30
7[b]	**Pd4**	64

[a] Reaction conditions: 4-Chlorobenzaldehyde (0.25 mmol), pyrrolidine (0.25 mmol), DMF 3 mL, catalyst (0.1 mol%), irradiated with white light (24 W) for 16 h under O_2 at rt.
[b] Open air.

Table 8
Solvent optimization for photo-oxidative amide synthesis[a].

SL No	Solvent	Yield %
1	ACN	68
2	DCM	48
3	MeOH	12
4	CHCl3	64
5	THF	50
6	DMF	62

[a] Reaction conditions: 4-Chlorobenzaldehyde (0.25 mmol), pyrrolidine (0.25 mmol), Solvent 3 mL, catalyst (0.1 mol%), irradiated with white light (24 W) for 16 h in open air.

oxidative amide synthesis was also examined (scheme 3). Notably, the Pd(II)–dipyrrinato complexes also proved competent for this transformation, under white light irradiation in an oxygen atmosphere. The reaction proceeded efficiently even under open air conditions, indicating that aerial oxygen is sufficient to sustain the oxidative amide synthesis (Table 6a).

To evaluate the catalyst loading, a study was performed (Table 6a), and it was found that only 0.1 mol% **Pd4** catalyst was needed for the photo-oxidative amide synthesis. After catalytic loading studies, catalyst optimization for the photo-oxidative amide synthesis was performed (Table 7). Among the Pd(II)dipyrrinato complexes, **Pd1–Pd3** showed only moderate activity, affording yields of 39%, 47%, and 38%, respectively. **Pd5** and **Pd6** were even less efficient, yielding only 29% and 30%, respectively. In contrast, **Pd4** again emerged as the most effective photocatalyst, providing a significantly improved yield of 63%. Notably, when the reaction was conducted under open-air conditions using atmospheric oxygen instead of an O_2 atmosphere, **Pd4** yielded a comparable 64%.

Solvent effects on the photo-oxidative amide synthesis were subsequently examined (Table 8). Among the solvents screened, acetonitrile provided the highest yield (68%) and proved to be the most effective medium for the transformation. $CHCl_3$ and DMF also supported good reactivity, affording 64% and 62% yields, respectively. Moderate efficiencies were observed in THF (50%) and DCM (48%), whereas MeOH led to a substantial decrease in product formation (12%), likely due to competitive quenching or catalyst deactivation. Overall, these results identify ACN as the optimal solvent for achieving efficient photo-oxidative C–N coupling under the **Pd4** catalytic system.

With the optimized catalytic conditions in hand, the substrate scope of the photo-oxidative amide synthesis was evaluated using a variety of substituted benzaldehydes and cyclic amines (Fig. 8). Halogen-substituted aldehydes under the standard conditions, gave **4a** (Cl, 68%), **4b** (I, 58%), and **4c** (Br, 61%) in moderate to good yields. Electron-donating substituents were also well tolerated, providing **4d** (Me, 68%) and **4e** (OMe, 70%). Strong electron-withdrawing groups, such as CN and NO_2, yielded excellent conversion, with products **4f** (CN, 84%) and **4g**(NO_2, 90%). Trifluoromethyl-containing substrates also gave excellent yields 72% for both **4h** and **4i**, respectively. Heteroaromatic and extended aromatic systems were compatible, producing **4j** (87%), and **4k** (75%). Polycyclic derivatives also underwent efficient coupling, affording **4l** (63%).

Additionally, piperidine, with choro, cyno and nitro substituted benzaldehyde as coupling partner, also gave products **4m** (60%), **4n** (65%) and **4o** (68%) respectively. While in case of morpholine with cyno and nitro substituted benzaldehyde producing **4p** (55%) and **4q** (53%) respectively. Overall, the method exhibits broad functional-group tolerance and effective photo-oxidative amide synthesis formation under white-light irradiation and ambient oxygen conditions. Photo-oxidative functionalization of tetrahydroisoquinoline was also achieved using Pd(II)dipyrrinato photocatalytic system. Initially catalyst loading studies identified 0.5 mol% **Pd4** as the optimal loading for these transformations. After catalyst loading, a systematic catalyst optimization and control experiment was carried out (Table 9). Among the catalyst series**, Pd1, Pd3, Pd5**, and **Pd6** exhibited modest reactivity, yielding 7%, 24%, 29%, and 36%, respectively. **Pd2** showed improved yield of 51%, whereas **Pd4** again showed the highest efficiency with a 72% yield, confirming it as the most effective photocatalyst for this transformation. Control experiments confirmed that light, oxygen, and a photocatalyst were needed for the reaction. Collectively, these optimizations demonstrate that **Pd4** (0.5 mol%), molecular oxygen, and photoirradiation are essential for the efficient oxidative functionalization of tetrahydroisoquinoline (scheme 4).

With the optimized reaction conditions, the substrate scope of the photo-oxidative functionalization of tetrahydroisoquinolines was examined (Fig. 9). A variety of *N*-aryl tetrahydroisoquinoline derivatives bearing electronically diverse substituents underwent smooth oxidation to furnish the corresponding nitro-functionalized products **6a–6g** in consistently good yields. Unsubstituted *N*-aryl substrate afforded product **6a** in 72% yield, while substrates bearing electron-donating groups such as amino and methyl provided **6b** and **6c** with 68% and 70% yield, respectively. Along with bromo substituents at different positions, compounds **6d, 6e,** and **6f** were obtained with yields of 70%, 71%, and 69%, respectively.

The reaction was also compatible with malononitrile as an electrophile in the presence of acetonitrile as solvent, under the same conditions. The photo-oxidative functionalization protocol was further extended to malononitrile as an electrophile under the optimized **Pd4** catalytic system (Fig. 10). In acetonitrile and under white-light irradiation in an O_2 atmosphere, a range of *N*-aryl tetrahydroisoquinolines showed functionalization to afford products **7a–7e** in good yields (61–75%). Overall, the results demonstrate that the **Pd4** catalyzed

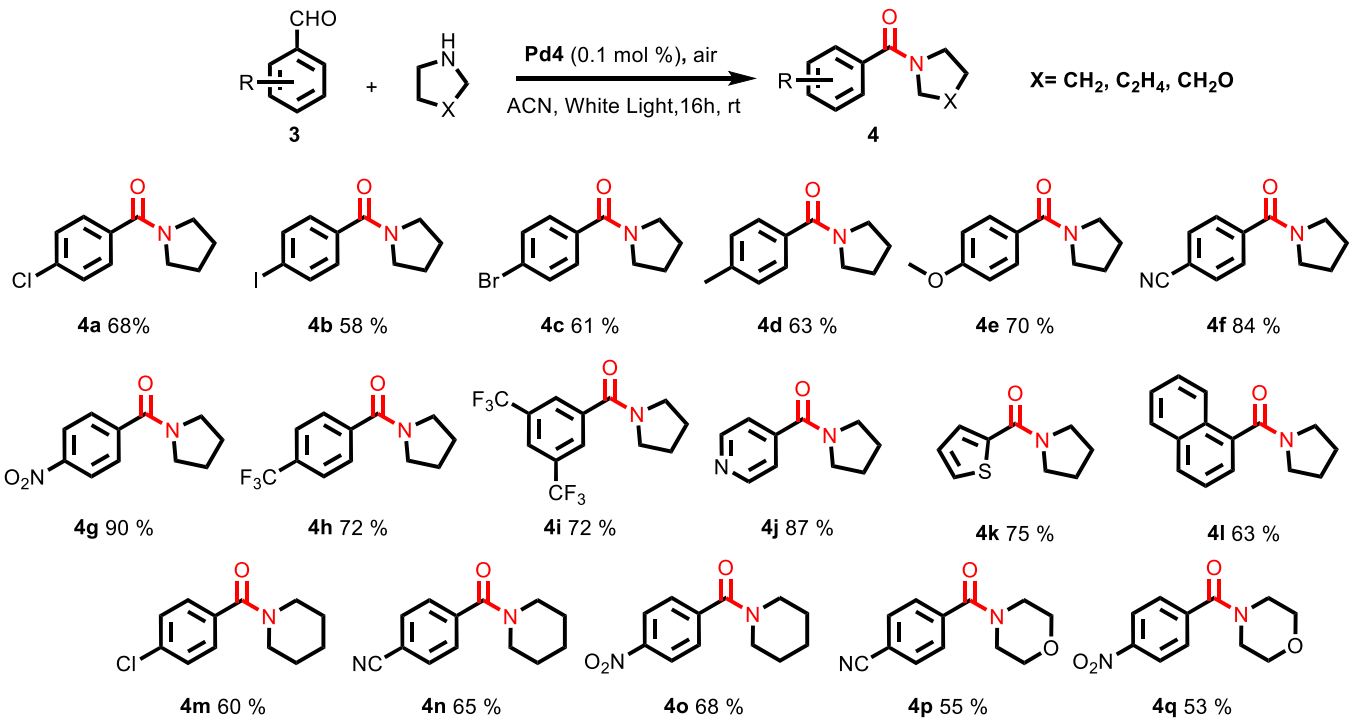

Fig. 8. Substrate scope of photo-oxidative amide synthesis.

Table 9
Reaction optimization for photo-oxidative functionalization of tetrahydroisoquinoline.[a.]

Sl No.	Catalyst	Yield[b] %
1	**Pd1**	7
2	**Pd2**	51
3	**Pd3**	24
4	**Pd4**	72
5	**Pd5**	29
6	**Pd6**	36
7[c]	**Pd4**	Trace
8[d]	-	Trace
9[e]	**Pd4**	Trace
10[f]	**Pd4**	13
11 *g*11[g]	**Pd4**	27

[a] Reaction conditions: *N*-phenyl-tetrahydroisoquinoline (0.25 mmol), Nitromethane 1 mL, catalyst (0.5 mol%), irradiated with white light (24 W) for 6 h in O_2.
[b] Yield was calculated by ^{1}H NMR using 1,3,5 trimethylbenzene (0.25 mmol) as an internal standard.
[c] No Light.
[d] No catalyst.
[e] Inert atmosphere.
[f] Nitromethane (0.5 mol) 2 ml ACN.
[g] Nitromethane (1 mol) 2 ml ACN.

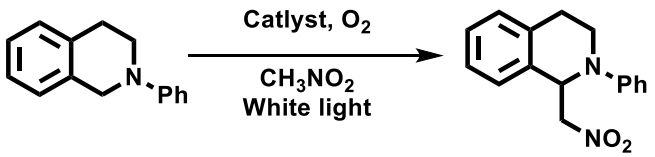

Scheme 4. General scheme of photo-oxidative functionalization of tetrahydroisoquinoline synthesis.

photo-oxidative protocol accommodates a wide range of functional groups, highlighting its robustness and broad synthetic applicability.

The comparative Tables 10–12 indicate that the Pd(II)dipyrrinato catalyst is highly competitive with established homogeneous photocatalysts. In the Witkop oxidation, although Rose Bengal provides slightly higher yield (92%), it requires higher loading (3 mol%) and longer time (45 h), whereas **Pd4** catalyst achieves 87% yield at only 0.05 mol% within 8 h under white LED irradiation. It also significantly outperforms $Ru(bpy)_3Cl_2$, Eosin Y, and Methylene blue. For photo-oxidative amidation and tetrahydroisoquinoline functionalization, the **Pd4** catalyst affords high yields (90% and 75%, respectively) under additive-free, white LED conditions, with shorter reaction times and low catalyst loading. Although some systems such as $Ir(ppy)_2(dtbbpy)PF_6$ deliver comparable yields, they often require higher loadings or specialized light sources [59–61]. Overall, the operational simplicity, low catalyst loading, and broad reactivity profile make this Pd system superior or strongly competitive among reported photocatalysts.

3. Conclusion

In summary, a series of Pd(II)dipyrrinato complexes were successfully synthesized and characterized. The Pd(II)dipyrrinato complexes exhibited strong visible-light absorption, high singlet oxygen quantum yield, and suitable redox potential. Among all the catalyst, **Pd4** exhibited the highest long-lived triplet excited state, followed by **Pd2**. These Pd(II)dipyrrinato complexes have been utilized as a photocatalyst under white light irradiation, for various oxidation reactions. **Pd4** gave superior photocatalytic performance and efficiently promoted Witkop oxidation, photo-oxidative amide synthesis, and oxidative functionalization of tetrahydroisoquinolines using molecular oxygen or aerial oxygen as an oxidant. In comparison to the reported photocatalysts, **Pd4** delivered comparable yields with significantly lower catalyst loading, shorter reaction times, and simple white-LED irradiation conditions across multiple oxidative transformations. The established protocol operates under mild conditions, displays broad substrate scope and good functional-group tolerance in these cases. Overall, this work establishes **Pd4** as a versatile and effective class of photocatalysts for sustainable aerobic oxidation reactions.

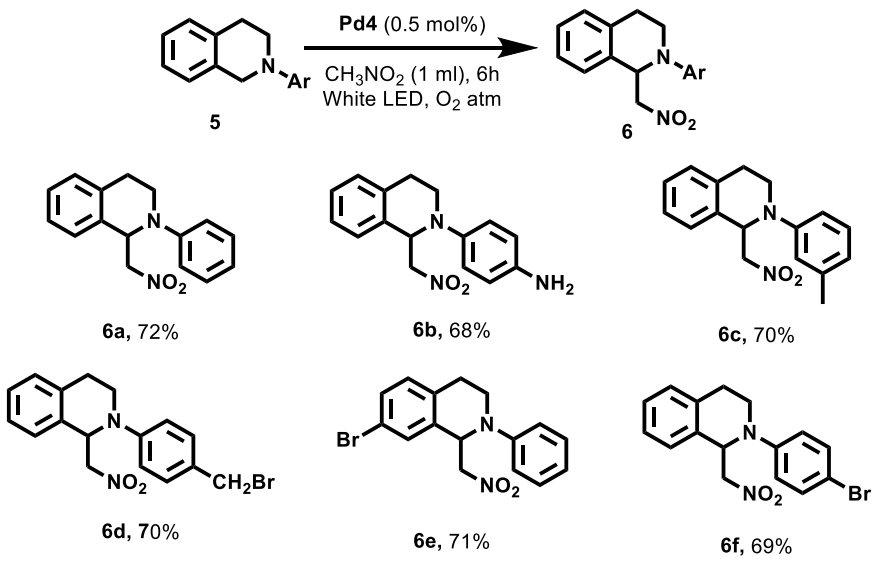

Fig. 9. Substrate scope of photo-oxidative functionalization of tetrahydroisoquinolines by nitromethane.

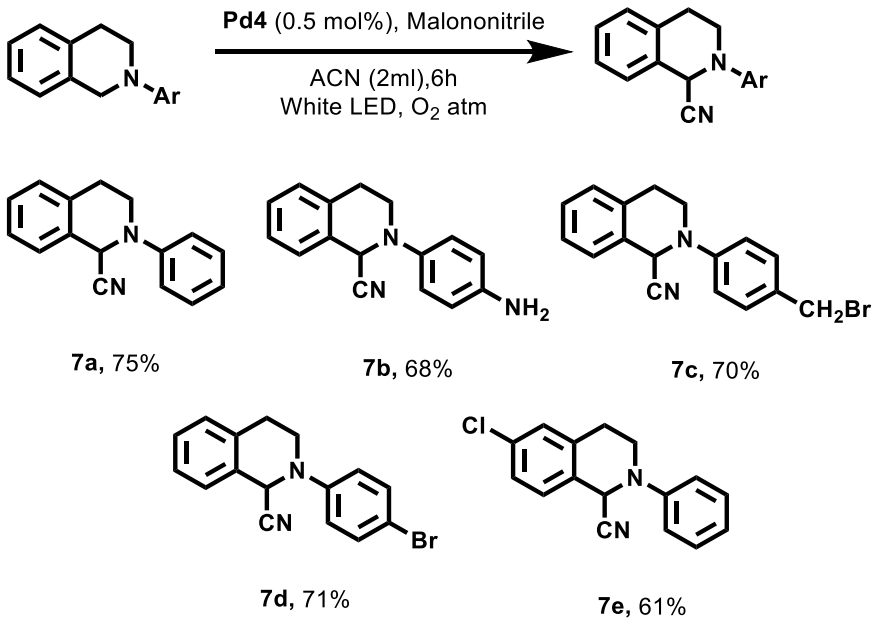

Fig. 10. Substrate scope of photo-oxidative functionalization of tetrahydroisoquinolines by malonitrile.

Table 10
Comparative table for Witkop oxidation between different homogenious photocatalyst.

Catalyst	Light	Mole %	Time	Additive	Yield %	TON	TOF	Ref
Rose Bengal	Blue (LED)	3	45 h	K_3PO_4	92	30.66	0.68	[51]
$Ru(bpy)_3Cl_2$	Blue (LED)	2	14 h	-	20	10	0.71	[11]
eosinY	White (LED)	5	24 h	-	17	3.4	0.14	[50]
Methylene blue	White (LED)	5	24 h	-	15	3	0.125	[50]
Crude chlorophyll	White (LED)	0.003	24 h	SDS	79	26,333.33	1097.22	[50]
meso-tetrakis-*p*-cyanophenyl Porphyrin	Blue (LED)	0.1	5 h	K_3PO_4	78	780	156	[52]
Re(I) Complex	Blue (LED)	0.25	4 h	K_3PO_4	79	316	79	[37]
Pd4 catalyst	White (LED)	0.05	8 h	K_3PO_4	87	1740	217.5	This work

CRediT authorship contribution statement

Shekhar Kumar: Writing – original draft, Software, Methodology, Investigation, Data curation, Conceptualization. **Yati:** Software, Data curation. **Samrita Sharma:** Visualization, Validation, Methodology. **Anirban Mondal:** Writing – review & editing, Software. **Iti Gupta:** Writing – review & editing, Supervision, Project administration, Funding acquisition, Conceptualization.

Table 11
Comparative table for photo-oxidative amide synthesis between different homogenious photocatalyst.

Catalyst	Light	Mole%	Time	Additive	Yield %	TON	TOF	Ref
$Ru(bpy)_3Cl_2$	Blue (LED)	2	20 h	CCl_3Br	66	33	1.65	[14]
	Blue (LED)	2	12 h	-	37	18.5	1.54	[31]
	Blue (LED)	1	24 h	^tBuOOH and NSC	85	85	3.54	[15]
$Ir[dF(CF_3)ppy]_2(dtbbpy)PF_6$	Blue (LED)	2	20 h	CCl_3Br	75	37.5	1.87	[14]
BODIPY	Blue (LED)	2	12 h	BHT	96	48	4	[31]
Methylene blue	Blue (LED)	2	12 h	-	16	8	0.66	[31]
Mn Based complex	UV-A	2	24 h	NaH	94	47	1.95	[32]
Pd4 catalyst	White (LED)	0.1	16 h	-	90	900	56.25	This work

Table 12
Comparative table for photo-oxidative functionalization of tetrahydroisoquinolines between different homogenious photocatalyst.

Catalyst	Light	Mole %	Time	Additive	Yield%	TON	TOF	Ref
Eosin Y	Green (LED)	2	10h	-	62	31	3.1	[59]
Rose Bengal	Green (LED)	5	72h	-	95	19	0.26	[60]
Chlorophyll	Red (LED)	2	24h	-	88	44	1.83	[61]
$Ir(ppy)_2(dtbbpy)PF_6$	White CFL	1	10h	-	92	92	9.2	[16]
$Ru(phen)_3$@InTATB	White CFL	0.2	48h	-	84	420	8.75	[17]
Pd4 catalyst	White (LED)	0.5	6h	-	75	150	25	This work

Declaration of competing interest

The authors declare that they have no known competing financial interests or personal relationships that could have appeared to influence the work reported in this paper.

Acknowledgements

Financial support from IIT Gandhinagar and CSIR, GoI (Grant No: 01/3132/23/EMR-II) is greatly acknowledged. SK thanks IIT Gandhinagar for the fellowship and infrastructural support. SS thanks DST, Government of India for INSPIRE fellowship (IF20283) and IIT Gandhinagar for the infrastructural support. YS thanks IIT Gandhinagar for the fellowship. AM acknowledges the Param Ananta for computational support.

Supplementary materials

Supplementary material associated with this article can be found, in the online version, at doi:10.1016/j.mcat.2026.116006.

Data availability

Data will be made available on request.

References

[1] D.A. Nicewicz, D.W.C. MacMillan, Merging photoredox catalysis with organocatalysis: the direct asymmetric alkylation of aldehydes, Science 322 (2008) 77–80, https://doi.org/10.1126/science.1161976.
[2] C.K. Prier, D.A. Rankic, D.W.C. MacMillan, Visible light photoredox catalysis with transition metal complexes: applications in organic synthesis, Chem. Rev. 113 (2013) 5322–5363, https://doi.org/10.1021/cr300503r.
[3] K.L. Skubi, T.R. Blum, T.P. Yoon, Dual catalysis strategies in photochemical synthesis, Chem. Rev. 116 (2016) 10035–10074, https://doi.org/10.1021/acs.chemrev.6b00018.
[4] F. Strieth-Kalthoff, M.J. James, M. Teders, L. Pitzer, F. Glorius, Energy transfer catalysis mediated by visible light: principles, applications, directions, Chem. Soc. Rev. 47 (2018) 7190–7202, https://doi.org/10.1039/C8CS00054A.
[5] a) B. Tang, F.X. Xiao, An overview of solar-driven photoelectrochemical CO_2 conversion to chemical fuels, ACS Catal. 12 (2022) 9023–9057, https://doi.org/10.1021/acscatal.2c01667;
b) P. Su, J.L. Liu, F.X. Xiao, Optimization of electron transfer pathways in atomically precise metal nanoclusters: catalyzing a leap in solar water oxidation, Chem. Sci. 17 (2026) 3300–3312, https://doi.org/10.1039/D5SC08806B.
[6] a) M.A. Ischay, M.E. Anzovino, J. Du, T.P. Yoon, Efficient visible light photocatalysis of [2+2] enone cycloadditions, J. Am. Chem. Soc. 130 (2008) 12886–12887, https://doi.org/10.1021/ja805387f;
b) Y.B. Li, F.X. Xiao, Surmounting the instability of atomically precise metal nanoclusters towards boosted photoredox organic transformation, Chem. Sci. 16 (2025) 2661–2672, https://doi.org/10.1039/D4SC06256F.
[7] M. Mentel, R. Breinbauer, The Witkop-Winterfeldt-oxidation of indoles, Curr. Org. Chem. 11 (2007) 159–176, https://doi.org/10.2174/138527207779316426.
[8] R. Curci, R. DiPrete, J.O. Edwards, G. Modena, Role of solvent in the oxidation of some organic compounds by peroxyacids, J. Org. Chem. 35 (1970) 740–745, https://doi.org/10.1021/jo00828a044.
[9] V.G. Shukla, P.D. Salgaonkar, K.G. Akamanchi, A. Mild, Chemoselective oxidation of sulfides to sulfoxides using *o*- iodoxybenzoic acid and tetraethylammonium bromide as catalyst, J. Org. Chem. 68 (2003) 5422–5425, https://doi.org/10.1021/jo034483b.
[10] Z. Xu, Z. Zhang, X. Yao, S. Li, L. Zhang, Green selective oxidation of substituted indoles catalyzed by CuCl, J. Org. Chem. 88 (2023) 4694–4703, https://doi.org/10.1021/acs.joc.3c00174.
[11] L.T. Cheng, S.Q. Luo, B.C. Hong, C.L. Chen, W.S. Li, G.H. Lee, Oxidative trimerization of indoles via water-assisted visible-light photoredox catalysis and the study of their anti-cancer activities, Org. Biomol. Chem. 18 (2020) 6247–6252, https://doi.org/10.1039/d0ob01298j.
[12] Y.-L. Li, A.-J. Li, S.-L. Huang, J.J. Vittal, G.Y. Yang, Polypyridyl Ru(ii) or cyclometalated Ir(iii) functionalized architectures for photocatalysis, Chem. Soc. Rev. 52 (2023) 4725–4754, https://doi.org/10.1039/D3CS00053B.
[13] O. Fayafrou, E. Lognon, C. Duhayon, J.B. Sortais, A. Monari, O. Baslé, Y. Canac, Photoluminescent ruthenium(ii) bipyridyl complexes containing phosphonium ylide ligands, Chem. Com. 60 (2024) 13602–13605, https://doi.org/10.1039/d4cc05050a.
[14] G. Pandey, S. Koley, R. Talukdar, P.K. Sahani, Cross-dehydrogenating coupling of aldehydes with amines/R-OTBS ethers by visible-light photoredox catalysis: synthesis of amides, esters, and ureas, Org. lett. 20 (2018) 5861–5865. https://pubs.acs.org/doi/10.1021/acs.orglett.8b02537.
[15] N. Iqbal, E.J. Cho, Visible-light-mediated synthesis of amides from aldehydes and amines via in situ acid chloride formation, J. Org. Chem. 81 (2016) 1905–1911. https://pubs.acs.org/doi/10.1021/acs.joc.5b02726.
[16] A.G. Condie, J.C. Gonzalez-Gomez, C.R. Stephenson, Visible-light photoredox catalysis: aza-Henry reactions via C− H functionalization, J. Am. Chem. Soc. 132 (2010) 1464–1465, https://doi.org/10.1021/ja909145y.
[17] J. Kim, S. Huh, Photoluminescence and photoredox catalytic properties of cationic Ru (ii) polypyridine complexes encapsulated within an InTATB metal–organic framework, Dalton Trans. 54 (2025) 14322–14330, https://doi.org/10.1039/D5DT01373A.
[18] A. Biffis, P. Centomo, A. Del Zotto, M. Zecca, Pd metal catalysts for cross-couplings and related reactions in the 21st century: a critical review, Chem. Rev. 118 (2018) 2249–2295, https://doi.org/10.1021/acs.chemrev.7b00443.
[19] N. Manav, A. Janaagal, I. Gupta, Unveiling new horizons: exploring rhenium and iridium dipyrrinato complexes as luminescent theranostic agents for phototherapy, Coord. Chem. Rev. 511 (2024) 215798, https://doi.org/10.1016/j.ccr.2024.215798.
[20] N. Manav, R. Singh, A. Janaagal, A.K.S. Yadav, V. Pandey, I. Gupta, Synthesis, computational and optical studies of tetraphenylethene-linked Pd(ii)dipyrrinato complexes, New J. Chem. 46 (2022) 19310–19321, https://doi.org/10.1039/D2NJ02719D.
[21] S.A. Baudron, Dipyrrin based metal complexes: reactivity and catalysis, Dalton Trans 49 (2020) 6161–6175, https://doi.org/10.1039/D0DT00884B.
[22] S. Kumar, K. Agarwal, A.Mondal Sanyam, I. Gupta, Harnessing solar power for oxidation of organic compounds by re(I)dipyrrinato complexes, Chem. Asian J. 19 (2024) e202400680, https://doi.org/10.1002/asia.202400680.

[23] S. Kumar, L. Devi, I. Gupta, Visible light assisted oxidation of organic compounds by iridium(iii)dipyrrinato complexes, New J. Chem. 49 (2025) 11080–11088, https://doi.org/10.1039/D5NJ01795E.

[24] J. Buckingham, K.H. Baggaley, A.D. Roberts, L.F. Szabo (Eds.), Dictionary of Alkaloids with CD-ROM, CRC Press, 2010, https://doi.org/10.1201/EBK1420077698.

[25] M. Bandini, A. Eichholzer, Catalytic functionalization of indoles in a new dimension, Angew. Chem. Int. Ed. 48 (2009) 9608–9644, https://doi.org/10.1002/anie.200901843.

[26] B.Karan Kumar Faheem, K.V.G. Chandra Sekhar, S. Chander, S. Kunjiappan, S. Murugesan, Medicinal chemistry perspectives of 1,2,3,4-tetrahydroisoquinoline analogs – biological activities and SAR studies, RSC Adv. 11 (2021) 12254–12287, https://doi.org/10.1039/D1RA01480C.

[27] J.P. Deore, M. De, Synthesis of biologically important tetrahydroisoquinoline (THIQ) motifs using quantum dot photocatalyst and evaluation of their anti-bacterial activity, Org. Biomol. Chem. 21 (2023) 9049–9053, https://doi.org/10.1039/D3OB01305G.

[28] J.M. Barbosa-Filho, M.R. Piuvezam, M.D. Moura, M.S. Silva, K.V.B. Lima, E.V.L. da-Cunha, I.M. Fechine, O.S. Takemura, Anti-inflammatory activity of alkaloids: a twenty-century review, Rev. Bras. Farmacogn. 16 (2006) 109–139, https://doi.org/10.1590/S0102-695X2006000100020.

[29] T. Cupido, J. Tulla-Puche, J. Spengler, F. Albericio, The synthesis of naturally occurring peptides and their analogs, Curr. Opin. Drug Discov. Devel. 10 (2007) 768–783.

[30] J.M. Humphrey, A.R. Chamberlin, Chemical synthesis of natural product peptides: coupling methods for the incorporation of noncoded amino acids into peptides, Chem. Rev. 97 (1997) 2243–2266, https://doi.org/10.1021/cr950005s.

[31] X.F. Wang, S.S. Yu, C. Wang, D. Xue, J. Xiao, BODIPY catalyzed amide synthesis promoted by BHT and air under visible light, Org. Biomol. Chem. 14 (2016) 7028–7037, https://doi.org/10.1039/C6OB00736H.

[32] A. Joshi, S. Kumari, S. Kundu, Photoredox (NN) Mn (I) catalysed acceptorless dehydrogenation: synthesis of amides, aldehydes and ketones, Adv. Synth. Catal. 364 (2022) 4371–4383, https://doi.org/10.1002/adsc.202201024.

[33] L.A. Mitscher, Bacterial topoisomerase inhibitors: quinolone and pyridone antibacterial agents, Chem. Rev. 105 (2005) 559–592, https://doi.org/10.1021/cr030101q.

[34] N. Llopis, P. Gisbert, A. Baeza, Oxidative cleavage of indoles mediated by urea hydrogen peroxide or H_2O_2 in polar solvents, Adv. Synth. Catal. 363 (2021) 3245–3249, https://doi.org/10.1002/adsc.202100214.

[35] G. Liao, F. Mei, Z. Chen, G. Yin, Lewis acid improved dioxygen activation by a non-heme iron(ii) complex towards tryptophan 2,3-dioxygenase activity for olefin oxygenation, Dalton Trans 51 (2022) 18024–18032, https://doi.org/10.1039/D2DT02769K.

[36] D.J.C. Constable, P.J. Dunn, J.D. Hayler, G.R. Humphrey Jr., J.L. Leazer, R. J. Linderman, K. Lorenz, J. Manley, B.A. Pearlman, A. Wells, A. Zaks, T.Y. Zhang, Key green chemistry research areas—A perspective from pharmaceutical manufacturers, Green Chem. 9 (2007) 411–420, https://doi.org/10.1039/B703488C.

[37] C. Bednarek, I. Wehl, N. Jung, U. Schepers, S. Bräse, The staudinger ligation, Chem. Rev. 120 (2020) 4301–4354, https://doi.org/10.1021/acs.chemrev.9b00665.

[38] H.F. Motiwala, M. Charaschanya, V.W. Day, J. Aubé, Remodeling and enhancing Schmidt reaction pathways in hexafluoroisopropanol, J. Org. Chem. 81 (2016) 1593–1609, https://doi.org/10.1021/acs.joc.5b02764.

[39] L. De Luca, G. Giacomelli, A. Porcheddu, Beckmann rearrangement of oximes under very mild conditions, J. Org. Chem. 67 (2002) 6272–6274, https://doi.org/10.1021/jo025960d.

[40] E. Boess, M. Van Hoof, S.L. Birdsall, M. Klussmann, Investigating the oxidation step in the $CuCl_2$ -catalyzed aerobic oxidative coupling reaction of *N* -aryl tetrahydroisoquinolines, J. Org. Chem. 85 (2020) 1972–1980, https://doi.org/10.1021/acs.joc.9b02707.

[41] T. Nobuta, N. Tada, A. Fujiya, A. Kariya, T. Miura, A. Itoh, Molecular iodine catalyzed cross-dehydrogenative coupling reaction between two sp^3 C–H bonds using hydrogen peroxide, Org. Lett. 15 (2013) 574–577, https://doi.org/10.1021/ol303389t.

[42] Z. Tashrifi, M. Mohammadi Khanaposhtani, B. Larijani, M. Mahdavi, C1-Functionalization of 1,2,3,4-tetrahydroisoquinolines (THIQs), Asian J. Org. Chem. 10 (2021) 2421–2439, https://doi.org/10.1002/ajoc.202100407.

[43] L. Devi, S. Sharma, K. Agarwal, I. Gupta, Light-assisted oxidative functionalization of indoles by *Re*-(I)Dipyrrinato catalyst, Appl. Organomet. Chem. 39 (2025) e70427, https://doi.org/10.1002/aoc.70427.

[44] D. Leow, Phenazinium salt-catalyzed aerobic oxidative amidation of aromatic aldehydes, Org. Lett. 16 (2014) 5812–5815, https://doi.org/10.1021/ol5029354.

[45] Z.S. Huang, Y.F. Wang, M.Y. Qi, M. Conte, Z.R. Tang, Y.J. Xu, Interface synergy of exposed oxygen vacancy and Pd Lewis acid sites enabling superior cooperative photoredox synthesis, Angew. Chem. 136 (2024) e202412707, https://doi.org/10.1002/anie.202412707.

[46] A. Hassan Tolba, M. Krupička, J. Chudoba, R. Cibulka, Amide bond formation via aerobic photooxidative coupling of aldehydes with amines catalyzed by a riboflavin derivative, Org. Lett. 23 (2021) 6825–6830, https://doi.org/10.1021/acs.orglett.1c02391.

[47] Y.-Z. Cheng, W. Ji, X. Wu, X. Ding, X.-F. Liu, B.-H. Han, Persistent radical cation sp^2 carbon-covalent organic framework for photocatalytic oxidative organic transformations, Appl. Catal. B-Environ. Energy 306 (2022) 121110, https://doi.org/10.1016/j.apcatb.2022.121110.

[48] C. Grundke, R.C. Silva, W.R. Kitzmann, K. Heinze, K.T. de Oliveira, T. Opatz, Photochemical α-aminonitrile synthesis using Zn-phthalocyanines as near-infrared photocatalysts, J. Org. Chem. 87 (2022) 5630–5642, https://doi.org/10.1021/acs.joc.1c03101.

[49] M.R. Patil, J. Shah, A.V. Kumar, A.R. Kapdi, Photo-induced sp^3 C−H bond arylation, cyanation and nitroalkylation of tetrahydroisoquinolines (THIQs) under visible light irradiation using a combination of NHPI and Rose Bengal, Chem. Asian J. 15 (2020) 4302–4306, https://doi.org/10.1002/asia.202000999.

[50] S. Banu, S. Choudhari, G. Patel, P.P. Yadav, Auto-tandem PET and EnT photocatalysis by crude chlorophyll under visible light towards the oxidative functionalization of indoles, Green Chem 23 (2021) 3039–3047, https://doi.org/10.1039/D1GC00138H.

[51] W. Schilling, Y. Zhang, D. Riemer, S. Das, Visible-light-mediated dearomatisation of indoles and pyrroles to pharmaceuticals and pesticides, Chem. Eur. J. 26 (2020) 390–395, https://doi.org/10.1002/chem.201904168.

[52] A. Janaagal, A. Jain, P. Maru, P. Chahal, T.J.D. Kumar, I. Gupta, Photocatalytic approach towards benzimidazole synthesis and oxidation of indoles by porphyrins, Chem. Asian J. 20 (2025) e00807, https://doi.org/10.1002/asia.202500807.

[53] P. Pushpanandan, Y.K. Maurya, T. Omagari, R. Hirosawa, M. Ishida, S. Mori, Y. Yasutake, S. Fukatsu, J. Mack, T. Nyokong, H. Furuta, Singly and doubly N-confused calix[4]phyrin organoplatinum(II) complexes as near-IR, Triplet Sensitizers Inorg. Chem. 56 (2017) 12572–12580, https://doi.org/10.1021/acs.inorgchem.7b02047.

[54] K. Rybicka-Jasińska, B. König, D. Gryko, Porphyrin-catalyzed photochemical C–H arylation of Heteroarenes Eur, J. Org. Chem. 15 (2017) 2104–2107, https://doi.org/10.1002/ejoc.201601518.

[55] M.J. Frisch, G.W. Trucks, H.B. Schlegel, G.E. Scuseria, M.A. Robb, J.R. Cheeseman, G. Scalmani, V. Barone, B. Mennucci, G.A. Petersson, et al., Gaussian 09, Revision E.01, Gaussian Inc, Wallingford, CT, 2009.

[56] F. Neese, The ORCA program system, WIREs Comput. Mol. Sci. 2 (2012) 73–78, https://doi.org/10.1002/wcms.81.

[57] M.D. Hanwell, D.E. Curtis, D.C. Lonie, T. Vandermeersch, E. Zurek, G.R. Hutchison, Avogadro: an advanced semantic chemical editor, visualization, and analysis platform, J. Cheminform. 4 (2012) 17, https://doi.org/10.1186/1758-2946-4-17.

[58] T. Lu, A comprehensive electron wavefunction analysis toolbox for chemists, Multiwfn, J. Chem. Phys. 161 (2024), https://doi.org/10.1063/5.0216272.

[59] D.P. Hari, B. König, Eosin Y catalyzed visible light oxidative C–C and C–P bond formation, Orga. Lett. 13 (2011) 3852–3855, https://doi.org/10.1021/ol201376v.

[60] Y. Pan, C.W. Kee, L. Chen, C.H. Tan, Dehydrogenative coupling reactions catalysed by Rose Bengal using visible light irradiation, Green Chem 13 (2011) 2682–2685, https://doi.org/10.1039/C1GC15489C.

[61] R. Zeng, P. Yan, B. Xu, Z.L. Jing, H. Liu, W.J. Lai, Q. Ouyang, Red-light-induced high-efficiency oxidation and functionalization of tetrahydroisoquinoline derivatives using chlorophyll as a photocatalyst, New J. Chem. 49 (2025) 4421–4426, https://doi.org/10.1039/D4NJ04864D.